Amanpreet Whan[1], *Harpreet Singh*[1], *Navdeep Malik*[1], *Anurag Balayan*[1], *Stuti Dwivedi*[1], *Anshul Sharma*[2], *Manoj Sahni*[3*], *Rajnish Mallick*[4]

OPTIMISING THE DESIGN OF AUXETIC CORE AIRFOIL FOR WING MORPHING APPLICATIONS

OPTIMIZACIJA U DIZAJNU AEROPROFILA SA JEZGROM OD AUKSETIČNIH MATERIJALA ZA PRIMENU KOD KRILA PROMENLJIVOG OBLIKA

Originalni naučni rad / Original scientific paper
Rad primljen / Paper received: 16.07.2024
https://doi.org/10.69644/ivk-2025-siA-0017

Adresa autora / Author's address:
[1)] Department of Mechanical Engineering, Thapar Institute of Engineering & Technology, Patiala, India
[2)] Department of Mechanical Engineering, National Institute of Technology, Hamirpur, India
[3)] Department of Mathematics, Pandit Deendayal Energy University, Gandhinagar, India [*]email: manojsahani117@gmail.com
[4)] School of Interdisciplinary Design and Innovation, Indian Institute of Information Technology Design and Manufacturing, IIIT DM Kancheepuram, Chennai, India

Keywords
- wing morphing
- trailing edge deflection
- smart auxetic structures
- genetic algorithm
- finite element analysis

Ključne reči
- krila promenljivog oblika
- savijanje vodeće ivice
- pametne auksetične konstrukcije
- genetički algoritam
- metoda konačnih elemenata

Abstract

Bird wings demonstrate phenomenal adaptation and aerodynamic performance across varied flight conditions. In contrast, conventional aircraft wings are designed for specific scenarios, limiting their adaptability. Therefore, the integration of smart cellular structures into morphing airfoils is crucial for furthering aircraft development. This entails integrating actuators, sensors, and innovative control systems to modernize aircraft engineering. One intriguing approach is adopting a re-entrant arrangement which exhibits a negative Poisson's ratio, popularly known as auxetic behaviour. This particular trait can bring substantial advantages to the morphing process. Morphing airfoils containing an auxetic core offer various benefits, including greater deformability, ease of control, variable stiffness, and improved stress tolerance. This research provides a novel approach by discovering the optimal re-entrant unit cell and extending its key advantage within the aerospace sector, focusing on achieving maximal wing trailing edge deflection. The paper explores the in-plane characteristics of a 2D re-entrant auxetic structure and evaluates the consequences of parameter changes on the structure's negative Poisson ratio. Through multi-objective optimisation employing a genetic algorithm, the study achieves a remarkable 99.53 % enhancement in Poisson's ratio and a substantial 158.70 % rise in the relative elastic modulus, as evaluated analytically. Further, Finite element analysis (FEA) of the Eppler 420 airfoil reveals that integrating the improved re-entrant core within the airfoil leads to a significant augmentation of 63.56 % in trailing edge deflection compared to past research. This research emphasizes the potential of adopting optimised re-entrant structures to boost the performance and adaptability of aircraft wings.

Izvod

Ptičija krila su primer adaptacije i aerodinamičkih performansi u različitim uslovima letenja. S druge strane, konvencionalna krila letelica se projektuju za specifične uslove, čime se ograničava njihova adaptabilnost. Stoga, integracija pametnih ćelijskih konstrukcija u aeroprofile promenljivog oblika je krucijalno za dalji razvoj letelica. Ovim se podrazumeva integracija pokretača, senzora i inovativnih sistema upravljanja radi modernizacije letelice. Interesantan pristup je usvajanje uvodnog rešenja, gde se obezbeđuje negativan Poasonov koeficijent, poznat kao auksetično ponašanje materijala. Ova posebna osobina može da doprinese značajnim prednostima u procesu promene oblika krila. Aeroprofili promenljivog oblika sa auksetičnim jezgrom daju razne prednosti, uključujući veće deformacije, lakoću upravljanja, promenljivu krutost i povećan dopušteni napon. Ova istraživanja daju novi pristup iznalaženjem optimalnog uvodnog elementa i proširivanjem ključnih prednosti u vazduhoplovnom sektoru, fokusiranjem ka postizanju maksimalnog savijanja vodeće ivice aeroprofila. Proučavaju se ravanske karakteristike 2D uvodne auksetične konstrukcije i daju procene posledica izmene parametara na negativni Poasonov koeficijent. Multi-objektivnom metodom optimizacije, uvođenjem genetičkog algoritma, postiže se izvanredno poboljšanje Poasonovog koeficijenta od 99.53 % i značajan porast relativnog modula elastičnosti od 158.70 %, dobijen analitički. Analiza konačnim elementima (FEA) Eppler 420 aeroprofila pokazuje da uvođenje poboljšanog uvodnog jezgra dovodi do značajne izmene (63.56 %) kod savijanja vodeće ivice, u poređenju sa ranijim istraživanjima. Ovim se podrazumeva potencijal u usvajanju optimizovanih uvodnih konstrukcija za poboljšanje performansi i adaptabilnosti krila letelice.

INTRODUCTION

The primary objective within any technical domain is to enhance present systems' efficiency or build novel ones with greater performance compared to their rivals. In the realm of aerospace engineering, this goal relates to optimising an air vehicle's aerodynamic, thermodynamic, and structural

layout. One viable technique to accomplish this is through the morphing concept. Morphing involves the continual changing of a structure's shape, permitting seamless alterations without the need for complex systems such as ailerons, flaps, slats, and spoilers. In other words, it refers to the continuous altering of a shape, i.e., different components remain stationary w.r.t. each other and flex as a unit upon actuation. In the context of aircraft wings, this entails the replacement of complex assemblies consisting of ailerons, flaps, slats, and spoilers with a monolithic structure capable of modulating its surface area and assembly seamlessly, disregarding the opening of gaps within itself and the main wing. This not only reduces sudden changes in the wing's shape and aerodynamic losses but also mitigates vibrations and noise within the aircraft's structure /1-3/.

The concept of morphing necessitates embedding a morphing structure within an aerodynamic enclosure, which is essential for its practical use in aerospace, notably wing morphing. A noteworthy requirement for morphing structures is their ability to undergo shape alterations in at least one of two ways: shifts in camber or modifications in surface area, needed for various components such as ailerons, slats, flaps, or winglets on aircraft wings /4/. Smart structures employ external actuators, integrated actuators, or self-actuating characteristics to enable form adjustment. These traits allow them to perceive different external stimuli (such as changes in velocity, pressure, or temperature) and respond in a controlled manner in real-time, making them perfect for aerodynamic encasements.

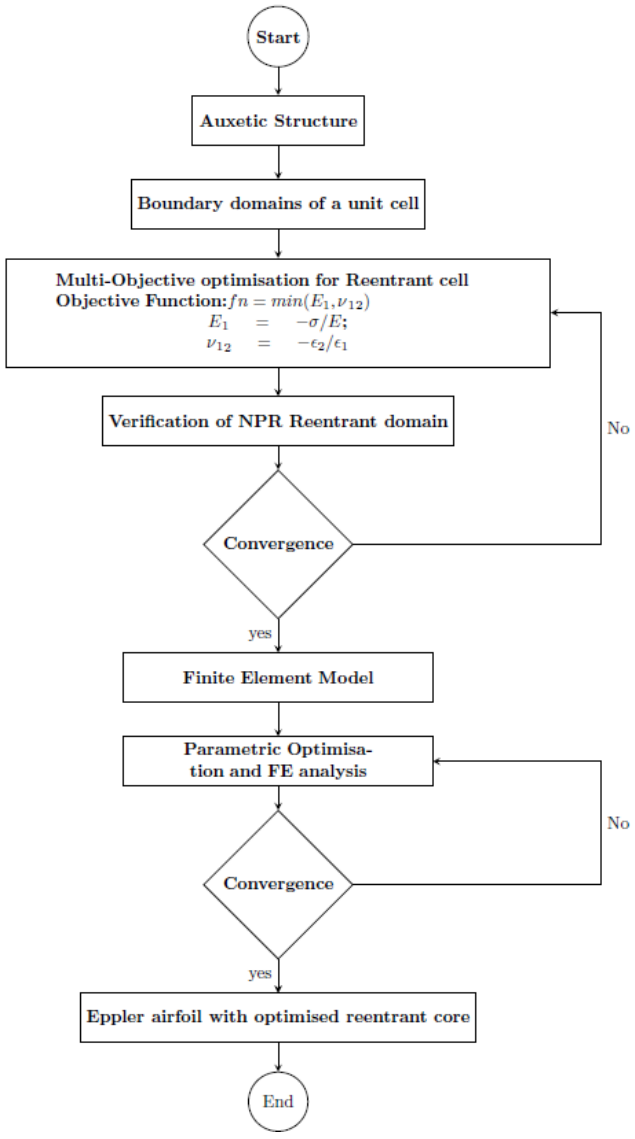

Figure 1. Flowchart indicates a two-step approach for designing an airfoil incorporating an optimised re-entrant core.

The integration of smart structures and adaptable technology in aircraft has unlocked prospects for revolutionary structural morphing concepts /5/. Morphing wings demand a flexible structure capable of controlled, compliant deformations while maintaining sufficient stiffness to withstand aerodynamic loads /6/. Cellular or auxetic structures, recognised for their enhanced mechanical properties and multifunctional attributes, are regarded as superior structural component designs. The structural auxetic qualities are driven by topology, where traits are governed by the geometry and shape of the particular cell that forms the structure. The geometry, shape, and accompanying attributes can be changed to fulfil unique application needs, or to obtain various functionality.

This research intends to delve into the subtleties of the auxetic re-entrant structure, employing analytical equations from literature. Additionally, the study applies optimisation techniques to design an optimal re-entrant structure that maximizes negative Poisson's ratio while enhancing the elastic modulus. Specifically, the research focuses on examining the performance of the Eppler 420 airfoil, which has a re-entrant core under aerostatic loading circumstances, assessing its load-bearing capacity and flexibility at the trailing edge. This analysis is then contrasted with an airfoil incorporating another re-entrant core but with optimal geometric parameters derived through a multi-objective optimisation approach.

MATERIALS AND METHODOLOGY

A two-step algorithm is developed to design an optimum auxetic re-entrant core integrated within the airfoil, aimed at achieving maximum trailing edge deflection. Initially, an analytical evaluation is undertaken to discover the influence of different geometrical parameters on the mechanical characteristics of the re-entrant structure. This assessment includes figuring out how variations in these parameters impact aspects such as directional Poisson's ratio and elastic moduli. The analytical examination relies on derived relationships from the pertinent published literature. The next phase involves parametrising the geometrical parameters associated with the re-entrant unit cell. This optimisation process is aided by a Genetic Algorithm, utilising the relationships derived from the Euler Bernoulli Beam theory elucidated by Hedayati et al. /13/. Figure 1 presents the flowchart of the proposed algorithm, outlining the subsequent stages as follows:

i. Selection of the geometrical parameters or domain of the auxetic re-entrant structure to be optimised.
ii. Execution of the multi-objective technique using MATLAB® to attain an optimised shape.

iii. Assessing the convergence of the unit cell concerning the Negative Poisson's Ratio (NPR).
iv. Development of a finite element model for a 3D airfoil incorporating the re-entrant core.
v. Conducting FEA utilising baseline and optimised geometrical parameters.
vi. Verification of the convergence of the finalised optimised design.

Material selection

The chosen material for the FEA investigation of a morphing airfoil is outlined in this section. While auxetic structures are commonly associated with metals or alloys, their utility extends to composites and polymers as well. For this analysis, aluminium alloy 6061 with specified properties, as detailed in Table 1, has been selected. Aluminium alloy 6061 is commonly employed in establishing a desirable balance between strength and weight, which is vital, notably in aerospace applications. The Al 6061 T6 variant, chosen for its superior machinability characteristics, has an enhanced response to anodising, and maintains equivalent corrosion resistance attributes. This material selection matches with the criteria for the intended application, ensuring optimal performance and structural integrity.

Table 1. Mechanical properties of aluminium alloy 6061.

Properties	Values	Units
Poisson's ratio (ν)	0.33	-
Density (ρ)	2770	kg/m^2
Young's modulus (E)	71000	MPa
Ultimate strength (σ_{ut})	310	MPa
Yield strength (σ_{yt})	280	MPa

Design of an airfoil integrating re-entrant core

In order to develop efficient compliant structures, it is crucial to strike a balance between rigidity and adaptability, which might be difficult due to opposing requirements. This section focuses on designing compliant cellular cores for a passive morphing airfoil, emphasizing a specific deformation mode while preserving acceptable stiffness against aerostatic loading. Our study investigates the re-entrant geometry, employing both baseline and optimised parameters for the core architecture. We undertake a comparative analysis focusing on the trailing edge deflections presented within the cores of the airfoil while simultaneously examining the maximum allowable strains and evaluating the local stresses of the material involved.

Re-entrant geometrical configuration and properties

In 1982, Gibson et al. identified the inverted hexagonal honeycomb, or so-called re-entrant structure, as one of the earliest configurations to possess auxetic behaviour and deliberately exploited it in a structural design. Almgren, in 1985, pioneered the adaptation of this structure from a two-dimensional to a three-dimensional model. This change was inspired by the aim to reach a homogeneous Poisson's ratio of –1 across all dimensions, /7/. The auxetic characteristics of re-entrant structures are predominantly determined by the angle between the ribs outlining the cellular structure. Figure 2 shows the geometric configuration of the re-entrant structure. The crucial geometric parameters encompass the vertical wall length (aligned with direction 2) denoted as *h*; the inclined wall length denoted by *l*; the angle formed between the vertical and inclined walls denoted as θ; the thickness of the cell wall denoted as *t*; the depth of the cell structure denoted as *d*; the horizontal dimension of the unit cell (along direction 1), referred to as *B*; and the vertical dimension of the unit cell (along direction 2) referred to as *H*. Formulated equations by various authors to calculate Poisson's ratios, elastic moduli, and shear modulus in the two in-plane directions of orthotropy of re-entrant hexagonal honeycomb structures are presented in Tables 2 and 3.

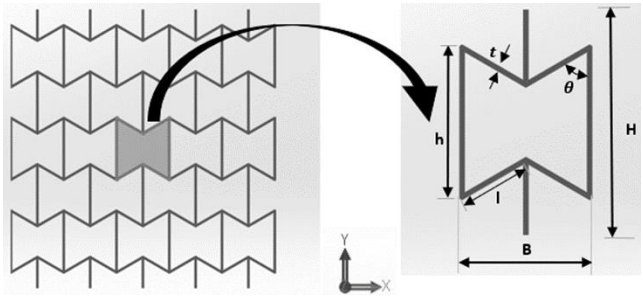

Figure 2. Auxetic lattice with re-entrant structure and its corresponding unit cell featuring geometrical parameters.

Table 2. Equations formulated by authors to determine in-plane elastic properties, as elastic moduli and Poisson ratio for re-entrant structures.

Gibson and Ashby /8, 9/

Poisson's ratio:

$$\nu_{12}=\frac{-B\cot\theta}{H} \quad (1), \qquad \nu_{21}=\frac{-H\tan\theta}{B} \quad (2)$$

Elasticity modulus:

$$E_1=8\frac{E_s t^3}{B^2 H}\frac{\sin\theta}{\cot^2\theta} \quad (3), \qquad E_2=8\frac{E_s t^3 H}{B^4}\sin\theta \quad (4)$$

Masters and Evans /10/

Poisson's ratios:

$$\nu_{12}=-\frac{B}{H}\frac{\frac{B^2}{4t^2 d\sin^2\theta}+2\nu_s+1}{\frac{B^2\cos\theta}{4t^2\sin^3\theta}+2(1+\nu_s)\cot\theta+\sin\theta\cos\theta} \quad (5), \qquad \nu_{21}=-\frac{H}{B}\frac{\frac{B^2}{4t^2 d\sin^2\theta}+2\nu_s+1}{\frac{B^2}{4t^2\sin\theta\cos\theta}+2(1+\nu_s)\tan\theta+\cot\theta+\frac{2H}{B\cos\theta}-\frac{2}{\sin\theta}} \quad (6)$$

Elastic modulus:

$$E_1=\frac{2E_s t}{H}\frac{1}{\frac{B^2\cos^2\theta}{4t^2\sin^3\theta}+2(1+\nu_s)\frac{\cos^2\theta}{\sin\theta}+\sin\theta} \quad (7), \qquad E_2=\frac{B^2}{2HE_s t}\frac{1}{\frac{B^2\cos^2\theta}{4t^2\sin\theta}+2(1+\nu_s)\sin\theta+2\frac{H}{B}+\frac{\cos^2\theta-2\cos\theta}{\sin\theta}} \quad (8)$$

Grima et al. /11/

Poisson's ratios:

$$\nu_{12}=-\frac{B}{H}\frac{\left\{\left[\frac{B}{2t\sin\theta}-\frac{1}{2}\left(\tan\frac{\theta}{2}-\cot\theta\right)\right]^2+1+2\nu_s\right\}\sin\theta\cos\theta}{\left[\frac{B}{2t\sin\theta}-\frac{1}{2}\left(\tan\frac{\theta}{2}-\cot\theta\right)\sin\theta\right]^2+2(1+\nu_s)\cos^2\theta+\sin^2\theta} \quad (9),$$

$$\nu_{21}=-\frac{H}{B}\frac{\left\{\left[\frac{B}{2t\sin\theta}-\frac{1}{2}\left(\tan\frac{\theta}{2}-\cot\theta\right)\right]^2+1+2\nu_s\right\}\sin\theta\cos\theta}{\left[\frac{B}{2t}-\frac{1}{2}\left(\tan\frac{\theta}{2}-\cot\theta\right)\sin\theta\right]^2+\frac{H+B\cot\theta+\frac{t}{2}\tan\frac{\theta}{2}}{\frac{B}{2\sin\theta}+\frac{t}{2}\left(\tan\frac{\theta}{2}-\cot\theta\right)}+\cos^2\theta+2(1+\nu_s)\sin^2\theta} \quad (10)$$

Elasticity modulus:

$$E_1=\frac{BE_st}{H}\frac{1}{\left[\frac{B}{2\sin\theta}-\frac{t}{2}\left(\tan\frac{\theta}{2}-\cot\theta\right)\right]\left[\frac{B}{2t}\cot\theta-\frac{1}{2}\left(\tan\frac{\theta}{2}-\cot\theta\right)\cos\theta\right]^2+2(1+\nu_s)\cos^2\theta+\sin^2\theta} \quad (11),$$

$$E_2=\frac{HE_st}{B}\frac{1}{\left[\frac{B}{2\sin\theta}-\frac{t}{2}\left(\tan\frac{\theta}{2}+\cot\theta\right)\right]\left\{\left[\frac{\frac{B}{\sin\theta}-t\left(\tan\frac{\theta}{2}-\cot\theta\right)}{\left(\frac{H}{2}-\frac{B}{2}\cot\theta\right)-\frac{t}{4}\tan\frac{\theta}{2}}+\cos^2\theta\right]\left[\frac{B}{2t}-\frac{1}{2}\left(\tan\frac{\theta}{2}+\cot\theta\right)\sin\theta\right]^2+2(1+\nu_s)\sin^2\theta\right\}} \quad (12)$$

Berinskii /12/

Poisson's ratio:

$$\nu_{12}=\frac{B}{H}\frac{2\left[1-\left(\frac{2t\sin\theta}{B}\right)^2\right]\sin\theta\cos\theta}{1+\left(\frac{2t\sin\theta}{B}\right)^2+\left[1-\left(\frac{2t\sin\theta}{B}\right)^2\right]\cos2\theta} \quad (13),$$

$$\nu_{21}=\frac{H}{B}\frac{2\left[1-\left(\frac{2t\cos\theta}{B}\right)^2\right]\sin\theta\cos\theta}{1+5\left(\frac{2t\cos\theta}{B}\right)^2-\left[1-\left(\frac{2t\sin\theta}{B}\right)^2\right]\cos2\theta} \quad (14)$$

Elasticity modulus:

$$E_1=\frac{2BE_s}{H}\frac{\left(\frac{2t\sin\theta}{B}\right)^3}{1+\left(\frac{2t\sin\theta}{B}\right)^2+\left[1-\left(\frac{2t\sin\theta}{B}\right)^2\right]\cos2\theta} \quad (15),$$

$$E_2=\frac{2HE_s}{B}\frac{\left(\frac{2t\sin\theta}{B}\right)^3}{1+5\left(\frac{2t\sin\theta}{B}\right)^2-\left[1-\left(\frac{2t\sin\theta}{B}\right)^2\right]\cos2\theta} \quad (16)$$

Table 3. Hedayati et al. formulated relationships to determine in-plane elastic properties such as Poisson's ratio and elastic moduli for re-entrant structures.

Hedayati et al. /13/

Euler Bernoulli beam theory:

Poisson's ratio:

$$\nu_{12}=\frac{B\sin2\theta(l^2-t^2)}{2H[(l^2-t^2)\cos^2\theta+t^2]} \quad (17),$$

$$\nu_{21}=\frac{Hl\sin^2\theta\cos\theta(l^2-t^2)}{Bl[(l^2-t^2)\sin^3\theta+t^2(l+H)\sin\theta-Bt^2\cos\theta]} \quad (18)$$

Elasticity modulus:

$$\left(\frac{E}{E_s}\right)_1=\frac{Bt^3}{Hl[(l^2-t^2)\cos^2\theta+t^2]} \quad (19),$$

$$\left(\frac{E}{E_s}\right)_2=\frac{Ht^3\sin\theta}{B[l(l^2-t^2)\sin^3\theta+t^2(l+H)\sin\theta-Bt^2\cos\theta]} \quad (20)$$

Timoshenko beam theory:

Poisson's ratio:

$$\nu_{12}=\frac{B(5l^2+7t^2+11t^2\nu_s)\sin2\theta}{H[(5l^2+7t^2+11t^2\nu_s)\cos^2\theta+(5l^2+7t^2+11t^2\nu_s)\cos2\theta]} \quad (21),$$

$$\nu_{21}=\frac{Hl\sin^2\theta\cos\theta(l^2+7t^2+11t^2\nu_s)}{Bl[(5l^2+7t^2+11t^2\nu_s)\sin^3\theta]+5t^2(l+H)\sin\theta-5Bt^2\cos\theta} \quad (22)$$

Elasticity modulus:

$$\left(\frac{E}{E_s}\right)_1=\frac{5Bt^3}{Hl[(5l^2+7t^2+11t^2\nu_s)\cos^2\theta+5t^2]} \quad (23),$$

$$\left(\frac{E}{E_s}\right)_2=\frac{5Ht^3\sin\theta}{B[l(5l^2+7t^2+11t^2\nu_s)\sin^3\theta+5t^2(l+H)\sin\theta-5Bt^2\cos\theta]} \quad (24)$$

Airfoil configurations

Chambered airfoils, mainly the Eppler 420 and Eppler 423, are extensively suggested in literature due to their substantial camber, resulting in a favourable lift-to-drag ratio.

Comparative tests reveal that the Eppler 420 outperforms the Eppler 423, creating more lift and less drag. Consequently, the Eppler 420 is chosen as the preferred airfoil for this study.

Based upon the unit cell geometry outlined in subsection *Re-entrant geometrical configuration and properties*, meso-structures are mapped onto an Eppler 420 airfoil profile, as represented in Fig. 3. The figure displays the airfoil configuration with an integrated re-entrant hexagonal honeycomb core. Additionally, Fig. 4 illustrates the deformation of the compliant core of the airfoil due to applied aerostatic load.

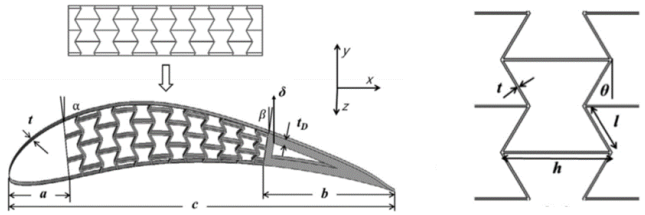

Figure 3. The Eppler 420 airfoil arrangement is integrated with a re-entrant auxetic core, /16/.

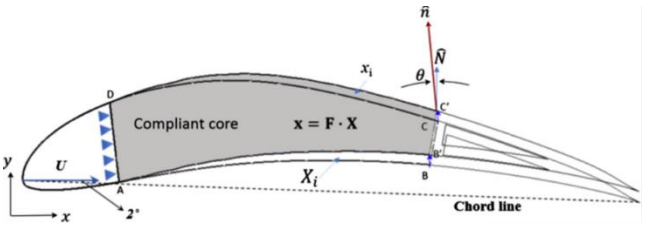

Figure 4. A visual representation demonstrating the deformation of a compliant core in response to an aerostatic load /16/.

Optimisation

This section applies a genetic algorithm for parametric optimisation targeted at strengthening the mechanical robustness of the re-entrant honeycomb structure. The emphasis is placed on optimising geometrical factors to attain superior mechanical properties. Optimisation is executed using the multi-objective genetic algorithm, particularly the *gamultiobj* toolbox, implemented in MATLAB®. To perform multi-objective optimisation on auxetic structures, we simultaneously address two vital objective functions, /14/. Utilising the MATLAB® *gamultiobj* tool, the geometric parameters of the unit cell are optimised by employing a Genetic Algorithm approach. This includes developing a comprehensive function encompassing the objectives, constraints, and design parameters within their respective domains /15/. Additionally, it entails initialising the initial population and chromosomes to ease the optimisation process, /17/.

In general, the *gamultiobj* tool aims to minimize the objective function. Therefore, objectives need to be clearly defined to obtain accurate results. The primary objective is to achieve a minimum negative Poisson's ratio and a maximum elastic modulus for the unit cell. This requires minimizing the negative modulus to maximize the objective and minimizing the Poisson's ratio below the null limit of 0. We utilise the Euler-Bernoulli beam theory formulations E_1 and ν_{12} as objective functions for optimisation. The chosen goal function and geometrical constraints for optimising it are delineated below:

$$\text{Objective}\begin{cases}\text{Maximise} E = fn(H,B,t,\theta)\\ \text{Minimise}\,\nu = fn(H,B,t,\theta)\end{cases}, \tag{25}$$

$$fn = \min(E_1,\nu_{12}), \tag{26}$$

$$E_1 = -\frac{\sigma}{E}, \tag{27}$$

$$\nu_{12} = -\frac{\varepsilon_2}{\varepsilon_1}, \tag{28}$$

$$\text{Subjected to:}\begin{cases}56.472 \le B \le 84.708\\ 30.584 \le H \le 45.876\\ 2.035 \le t \le 3.048\\ -40 \le \theta \le -25\end{cases}. \tag{29}$$

CAD and finite element modelling

To commence structural or Finite Element Analysis (FEA), the initial stage includes designing a CAD model. For our study, we utilised SolidWorks® 2018 to create a unit cell and then map the auxetic re-entrant core within an Eppler 420 airfoil. Figure 5 illustrates the CAD design process for the Eppler 420, featuring the re-entrant core. The geometrical configuration of the Eppler 420 airfoil and normal re-entrant core, as illustrated in Fig. 6, is based on the work of Heo and Kim, /16/. Upon completion of CAD modelling, all components are exported as Step files (.stp) since most FEA software accepts this format seamlessly. Subsequently, the optimised auxetic unit cell underwent validation, and its performance is verified by simulating a 3D airfoil incorporating an optimised re-entrant core using ANSYS software. The mechanical response under axial loading is studied employing the ANSYS® static structural module, a frequently applied tool for such assessments.

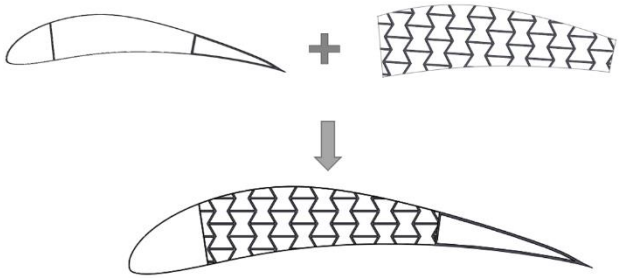

Figure 5. The process undertaken to design Eppler 420 airfoil embedded with re-entrant core.

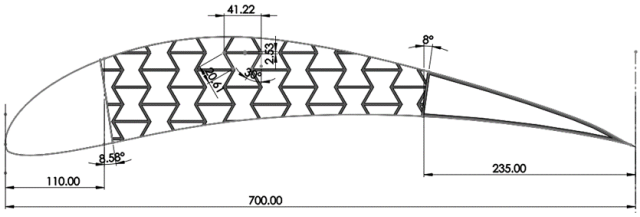

Figure 6. Geometric dimensions for the Eppler 420 airfoil are provided along with the re-entrant core, /7/.

RESULTS AND DISCUSSIONS

Analytical results

Analytical investigation focuses on determining in-plane mechanical properties, specifically the elastic modulus and Poisson's ratio. To ensure methodological coherence and enable comparative research, we modified Montgomery et al. strategy by utilising modified equations and dimensional parameters of the re-entrant unit cell, /18/. This allows for a complete comparison of mathematical expressions presented by various researchers. The chosen geometric unit cell has dimensions of $B{\cdot}H$ = 1·1 unit length, featuring a wall depth

thickness of d = 0.5 units and a consistent thickness of t = 0.05 units. We utilised an aluminium alloy with an elastic modulus of 71000 MPa and Poisson's ratio of 0.33. Employing MATLAB®, the effect of altering the angle between internal ribs ranging from 45° to 135° (where the angle is represented as 90 – θ) on mechanical properties is evaluated and the results are presented in Figs. 7-10.

Figure 7 exhibits the plotted Poisson's ratio ν_{12} curves showing full overlap among analytical formulations by diverse authors. However, for ν_{12}, the depicted curves in Fig. 8 indicate an analogous pattern except for formulations of Gibsons and Ashby. Notably, the ν_{12} curve tends towards infinity at θ = 90°. The primary reason behind this deviation in literature is that the author only considered bending as a deformation mechanism of re-entrant honeycombs and neglected another critical phenomenon, such as hinging and stretching. In accordance with the Gibson formulation, the elastic modulus in the x-direction exhibits asymptotic variation. Conversely, formulations proposed by other authors for E_1 and E_2 exhibit close agreement across a range of theta variations (see Figs. 9 and 10).

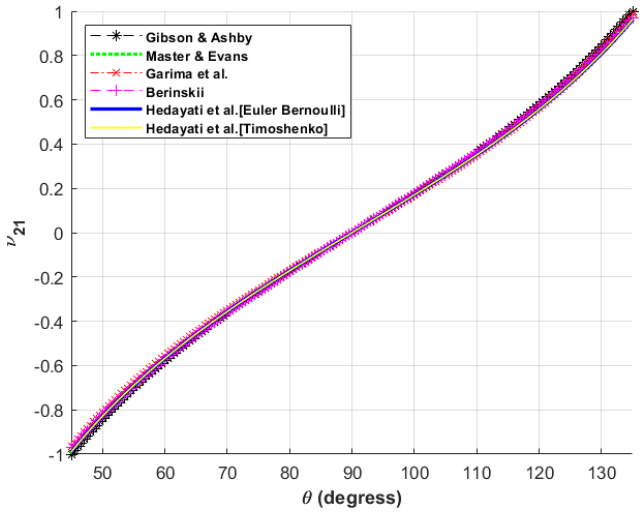

Figure 7. Comparison of Poisson's ratios ν_{21} with θ proposed by different authors for analysing re-entrant auxetic configurations.

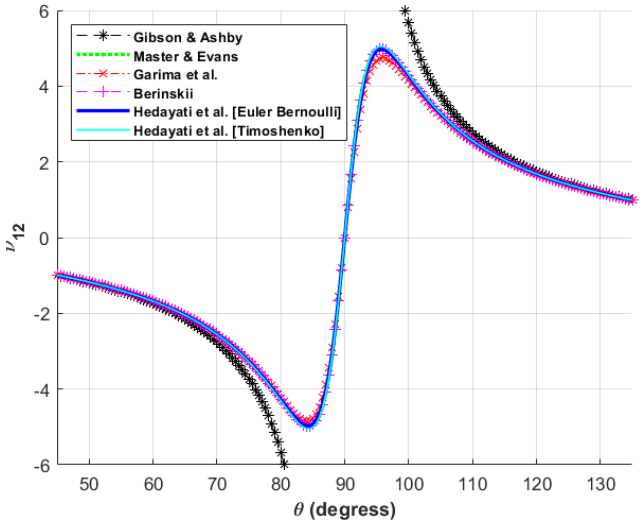

Figure 8. Comparison of Poisson's ratios ν_{12} with θ proposed by different authors for analysing re-entrant auxetic configurations.

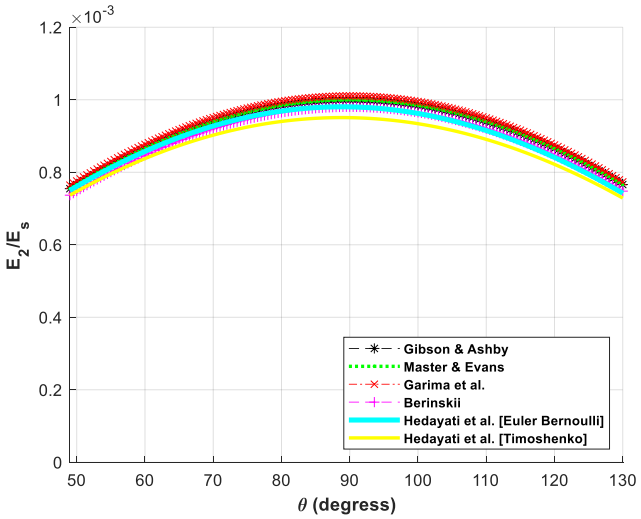

Figure 9. Comparison of the relative elastic moduli E_2/E_s with variable θ proposed by different authors for analysing re-entrant auxetic configurations.

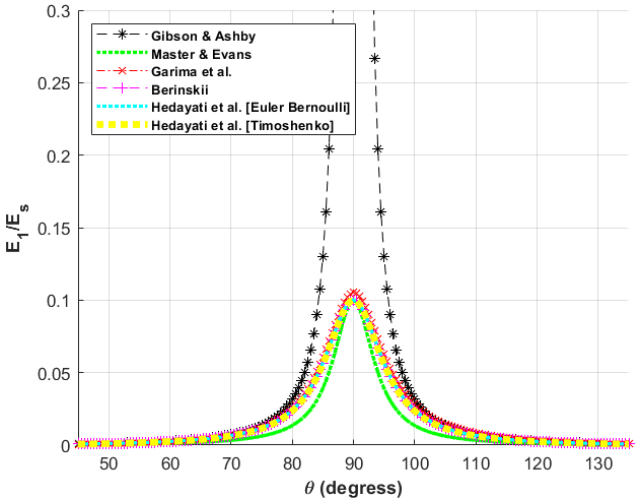

Figure 10. Comparison of the relative elastic moduli E_1/E_s with variable θ proposed by different authors for analysing re-entrant auxetic configurations.

Optimisation results

The optimisation task entails addressing two separate objective functions efficiently, utilising a single-objective optimisation approach. This is achieved by amalgamating both functions into a single multiobjective function. Utilising the *gamultiobj* toolbox generated roughly 8000 possible solutions, with Poisson's ratio extending from –0.8 to –2.8, and the relative elastic moduli ranging from 0.004 to 0.0017, as depicted in Fig. 11. The optimisation attempts to develop a structure that minimizes negative Poisson's ratio while demonstrating a high relative modulus to sustain substantial aerodynamic and structural loads when integrated into the wing auxetic core.

To identify the optimal configuration of the re-entrant unit cell configuration, the targeted ranges for Poisson's ratio and relative modulus are adjusted to –3 to –1.4 and 0.008 to 0.009, respectively. Figure 12 emphasizes the selected optimal spot for achieving maximum trailing edge displacement for the airfoil. Additionally, Table 4 documents the baseline

and optimised parameters for re-entrant parameters obtained alongside objective functions. Table 4 further showcases that upon optimising geometric parameters, there has been a notable enhancement in Poisson's ratio ν_{12} and relative elastic modulus E_1/E_s, with increments of 99.53 % and 158.70 %, respectively.

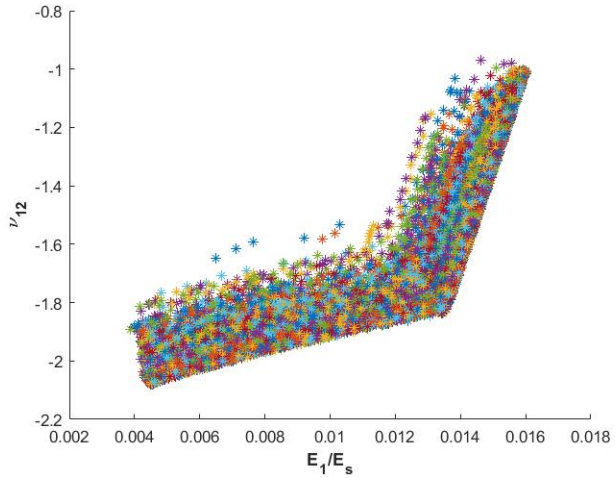

Figure 11. Pareto front illustrating feasible solutions with optimised objective functions, including Poisson's ratio ν_{12} and relative elastic moduli E_1/E_s.

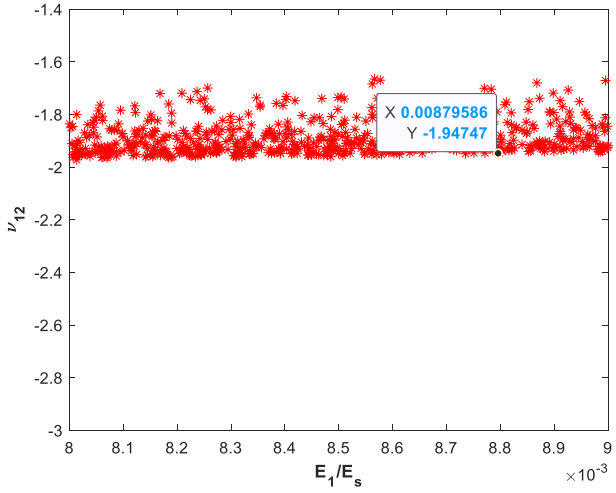

Figure 12. Chosen optimal point signifies optimal values for objective functions.

Table 4. Outcomes of objective functions employing both baseline and optimised geometrical parameters of re-entrant auxetic structures.

Baseline parameters				Objective functions	
B (mm)	H (mm)	t (mm)	θ (°)	ν_{12}	E_1/E_s
70.59	38.23	2.53	–30	–0.9760	0.0034
Optimal parameters				Optimised objective functions	
84.629	30.614	2.592	–39.981	–1.9475	0.00879

FEA analysis

Computational analysis of Eppler 420 airfoil incorporating a re-entrant core, employing both baseline and optimised unit cell configurations, is conducted utilising ANSYS® software platform. The static structural module is employed to calculate the maximum trailing edge deflection. After importing the respective CAD models into ANSYS, the models are meshed with an element size of 3 mm, and boundary constraints are applied to carry out the simulation as shown in Fig. 13.

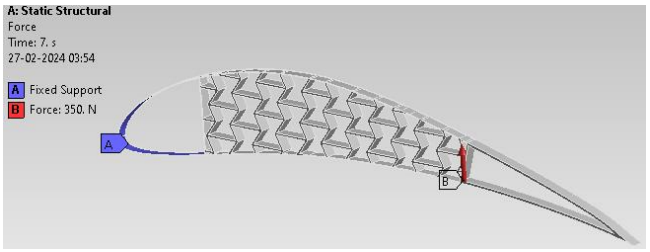

Figure 13. Assigned boundary constraints to conduct structural analysis to determine trailing edge deflection.

To evaluate the deflection of the trailing edge of the Eppler 420 airfoil integrated with the re-entrant core, a series of aerostatic loads ranging from 0 to 350 N are applied incrementally in steps of 50 N. The results obtained for the 350 N case are depicted in Fig. 13, while the incremental outcomes for maximum deflection are recorded in Table 5. As depicted in Figs. 14 and 15, the airfoil equipped with a conventional core exhibits a maximum trailing edge deflection of roughly 4.7 mm when subjected to an aerostatic load of 350 N. In contrast, the airfoil with the optimised core is approximately 7.7 mm. This indicates a 63.56 % improvement compared to the former case.

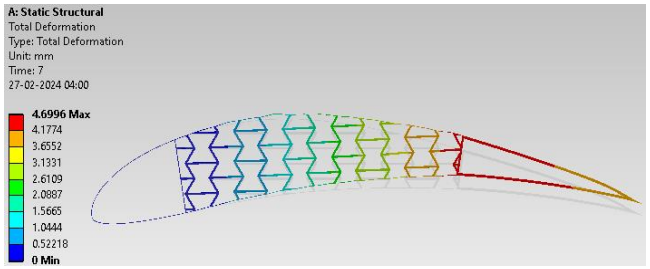

Figure 14. Deformation results of Eppler airfoil embedded with normal re-entrant core when subjected to an aerostatic load of 350 N.

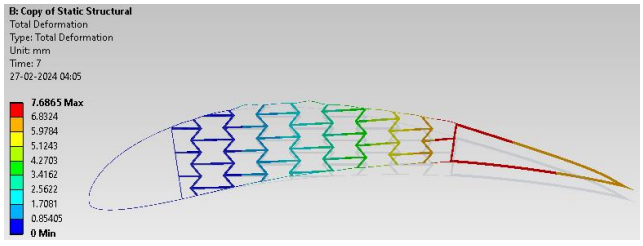

Figure 15. Deformation results of Eppler airfoil embedded with optimised re-entrant core when subjected to an aerostatic load of 350 N.

Table 5. Incremental outcomes for the maximum trailing edge deflection of Eppler 420 airfoil integrated with re-entrant core.

Load (N)	Deflection of trailing edge with normal core (mm)	Deflection of trailing edge with optimised core (mm)	Deflection improvement (%)
0	-	-	-
50	0.6612	1.0088	52.58
100	1.3226	2.0271	53.26
150	1.9856	3.0638	54.30
200	2.6516	4.1326	55.85
250	3.3232	5.2526	58.05
300	1.0037	6.4394	60.84
350	4.6996	7.6865	63.56

CONCLUSIONS

This study aims to design an optimal re-entrant unit cell with improved negative Poisson's ratio and elastic modulus to be embedded into an airfoil core. The main goal is to replace the complex assembly of a traditional aircraft wing, including ailerons, flaps, slats, and spoilers, with a monolithic structure. This structure is expected to endure considerable aerodynamic loads throughout varied flight regimes while minimizing drag losses and overall weight, thereby reducing emissions and manufacturing costs.

The research dives into assessments of analytical formulations by different authors concerning the in-plane elastic properties, namely Poisson's ratio and elastic modulus, examined for a re-entrant unit cell. With the angle between the ribs recognised as the key determinant of auxetic behaviour, the elastic properties are plotted for a range of varying angles (θ). Employing the *gamultiobj* toolbox in MATLAB®, optimisation attempts have been performed to discover the impact of angle and other parameters, thereby identifying optimal geometrical parameters for the unit cell. The optimal parameters resulted in an approximate 99.53 % increase in Poisson's ratio and a substantial 158.70 % augmentation in the relative elastic modulus, as determined analytically.

Finite element analysis was later performed to probe the maximum deflection of the trailing edge of the Eppler 420 airfoil under an incremental aerostatic load of 350 N applied in 50 N increments, encompassing both standard and optimised re-entrant cores. Analysis revealed that employing an optimised re-entrant core with refined geometrical parameters led to a significant augmentation of 63.56 % compared to utilising a standard re-entrant core.

ACKNOWLEDGEMENT

This work is financially assisted by the Science and Engineering Research Board (SERB), DST, India, under the MATRICS Scheme, File number: MTR/2022/001029 and also File number MTR/2023/000835.

REFERENCES

1. Mallick, R., Ganguli, R., Bhat, M.S. (2014), *An experimental and numerical study of piezoceramic actuator hysteresis in helicopter active vibration control*, Proc. Instit. Mech. Eng., Part G: J Aerosp. Eng. 228(5): 690-705. doi: 10.1177/0954410013478254
2. Mallick, R., Ganguli, R., Bhat, M.S. (2014), *A feasibility study of a post-buckled beam for actuating helicopter trailing edge flap*, Acta Mech. 225: 2783-2787. doi: 10.1007/s00707-014-1215-0
3. Wiggins, L., Stubbs, M., Johnston, C., et al. (2004), *A design and analysis of a morphing hyper-elliptic cambered span (HECS) wing*, In: 45th AIAA/ASME/ASCE/AHS/ASC Structures, Struct. Dyn. & Mater. Conf., Palm Springs, CA, 2004, Publ. AIAA-2008-1885.
4. Thill, C.L., Etches, J., Bond, I., et al. (2008), *Morphing skins*, The Aeronaut. J, 112(1129): 117-139. doi: 10.1017/S0001924000002062
5. McGowan, A.M.R., Cox, D.E., Lazos, B.S., et al. (2003), *Biologically inspired technologies in NASA's morphing project*, In: Proc. SPIE Vol.5051, Smart Structures and Materials 2003: Electroactive Polymer Actuators and Devices (EAPAD), San Diego, CA, 2003, SPIE. doi: 10.1117/12.484714
6. Spadoni, A., Ruzzene, M. (2007), *Numerical and experimental analysis of the static compliance of chiral truss-core airfoils*, J Mech. Mater. Struct. 2(5): 965-981. doi: 10.2140/jomms.2007.2.965
7. Almgren, R.F. (1985), *An isotropic three-dimensional structure with Poisson's ratio = -1*, J Elast. 15: 427-430. doi: 10.1007/BF0004253
8. Gibson, L.J., Ashby, M.F., Schajer, G.S., Robertson, C.I. (1982), *The mechanics of two-dimensional cellular materials*, In: Proc. Royal Soc. London, A: Math. Phys. Sci. 382(1782): 25-42. doi: 10.1098/rspa.1982.0087
9. Gibson, L.J. (2003), *Cellular solids*, MRS Bulletin, 28(4): 270-274. doi: 10.1557/mrs2003.79
10. Masters, I.G., Evans, K.E. (1996), *Models for the elastic deformation of honeycombs*, Compos. Struct. 35(4): 403-422. doi: 10.1016/S0263-8223(96)00054-2
11. Grima, J.N., Attard, D., Ellul, B., Gatt, R. (2011), *An improved analytical model for the elastic constants of auxetic and conventional hexagonal honeycombs*, Cell. Polym. 30(6): 287-310. doi: 10.1177/026248931103000602
12. Berinskii, I.E. (2018), *In-plane elastic properties of auxetic multilattices*, Smart Mater. Struct. 27(7): 075012. doi: 10.1088/1361-665X/aac292
13. Hedayati, R., Yousefi, A., Dezaki, M.L., Bodaghi, M. (2023), *Analytical relationships for 2D Re-entrant auxetic metamaterials: An application to 3D printing flexible implants*, J Mech. Behav. Biomed. Mater. 143: 105938. doi: 10.1016/j.jmbbm.2023.105938
14. Mallick, R., Ganguli, R., Kumar, R. (2017), *Optimal design of a smart post-buckled beam actuator using bat algorithm: simulations and experiments*, Smart Mater. Struct. 26(5): 055014. doi: 10.1088/1361-665X/aa6631
15. Mallick, R., Ganguli, R. (2016), *Optimal sizing of trailing edge flaps for helicopter vibration reduction: A response surface approach*, J Aerospace Sci. Technol. 68(3): 204-217. doi: 10.61653/joast.v68i3.2016.336
16. Heo, H., Ju, J., Kim, D.-M. (2013), *Compliant cellular structures: Application to a passive morphing airfoil*, Compos. Struct. 106: 560-569. doi: 10.1016/j.compstruct.2013.07.013
17. Padia, M., Sharma, P. (2022), *Design and development of auxetic structure using a two-step hybrid optimization technique*, Adv. Mater. Proc. Technol. 8(supp3): 1768-1784. doi: 10.1080/2374068X.2021.1959089
18. Montgomery-Liljeroth, E., Schievano, S., Burriesci, G. (2023), *Elastic properties of 2D auxetic honeycomb structures- a review*, Appl. Mater. Today, 30: 101722. doi: 10.1016/j.apmt.2022.101722